Supporting Information

Lin et al. 10.1073/pnas.1217113109

SI Materials and Methods

Biochemical Measurements in Cultured Cells. Biochemical measurements in fibroblasts were performed on mitochondria isolated from 2×10^9 cells as described (1, 2). Respiration was measured in freshly isolated mitochondria using a Clark-type electrode (Hansatech Instruments/PP Systems) (1).

ATP synthesis was measured in digitonin-permeabilized cells using the luciferase/luciferin system (3). Luminescence was measured for using a NOVOStar fluorimeter (BMG Labtech).

ROS production was determined using carboxy-H_2 2′,7′-dichlorofluorescein diacetate (DCFDA) (Invitrogen). Cells were incubated in media supplemented with 8 μM carboxy-H_2DCFDA, and fluorescence was monitored for 1 h at 37 °C at 485-nm excitation and 530-nm emission.

Electroretinography. Scotopic and photopic ERGs were performed using a 0.01 and 1 cd·s/m^2 flash stimulus and a 10 cd·s/m^2 and 20-Hz flicker stimulus, respectively. Mice were dark-adapted 12 h, and ERG recordings were performed using the Espion ERG Diagnosys system (Diagnosys). Mouse pupils were dilated with drops of AK-Pentolate (10 mg·mL^{-1} cyclopentolate hydrochloride ophthalmic solution) and AK-Dilate (1 mg·mL^{-1} phenylephrine hydochloride ophthalmic solution) (Akorn Inc., Lake Forest, IL). Animals were anesthetized with a ketamine (75 mg·kg^{-1}), and a dexmedetomidine (1.0 mg·kg^{-1}) mixture was administered intraperitoneally. Celluvisc was placed on the eyes, followed by surface electrodes. ERGs were recorded while the body temperature was maintained using a heating pad.

Optokinetic Analyses. Fourteen-month-old mice were placed inside a rodent OptoMotry System (CerebralMechanics) testing chamber. Visual acuity was determined by a yes/no scoring of recognition of black and white bars. Each test was conducted until the visual-acuity threshold was determined for each eye using a step-wise ladder system. The alternating white and black bars were set to 100% contrast and rotated at a constant rate.

Histology and Ultrastructural Analysis. Mouse eyes were fixed in half Karnovsky's fixative (2% paraformaldehyde and 2.5% glutaraldehyde) (4). For axonal counts, eyes were postfixed with 2% osmium tetroxide. *En bloc* staining was performed using 1% uranyl acetate. A PELCO Eponate kit (Ted Pella) was used for final epoxy resin embedding. One-micron sections were stained with 1% paraphenylenediamine and examined with a Zeiss Axioskop light microscope attached to a SPOT 7.3 three-shot color camera (Carl Zeiss), using a 100× objective lens at five points in each nerve. One picture in each set was excluded based on highest degree of longitudinally arranged axonal fibers. The nerves in the four remaining pictures were manually counted.

For transmission EM, 60- to 70-nm sections were prepared from postfixed optic nerve embedded in epoxy resin, mounted on 200-mesh grids, and evaluated using a transmission electron microscope (JEOL) (4). Twenty images were captured at 2,500× magnification from a single grid. Axons were included for evaluation if the entirety of the axoplasm was visible. Mitochondrial morphology was characterized based on cristae density and distribution.

Isolation of Mouse Mitochondria, Submitochondrial Particles, and Synaptosomes. Freshly minced liver was homogenized in H buffer [225 mM mannitol, 75 mM sucrose, 10 mM 3-(*N*-morpholino) propanesulfonic acid (Mops), 1 mM EGTA, 0.2% BSA (pH 7.4) at 4 °C], the homogenate was centrifuged at 500 × *g* for 10 min at 4 °C, and the resulting supernatant was centrifuged for another 5 min at 500 × *g*. The heavy mitochondrial fraction was recovered by centrifugation for 10 min at 3,000 × *g*. For mitochondria isolated for complex I activity, 10 mM Mops (pH 7.4) was used in place of homogenization buffer for the first washing to reduce rotenone insensitive activity.

Uncoupled submitochondrial particles were isolated from liver mitochondria (5). Nonsynaptic brain mitochondria were isolated using a discontinuous Percoll gradient by the method of Sims and Anderson (6). Synaptosomes were isolated from mouse forebrains as described previously (7, 8).

Complex I Activity Assays. NADH:coenzyme Q_1 oxidoreductase activity was determined with alamethicin-permeabilized liver mitochondria as described previously (9, 10). NADH:ferricyanide oxidoreductase assays were performed similarly using 2 mM potassium ferricyanide in place of coenzyme Q_1.

Oxygen Consumption of Isolated Mitochondria and Synaptosomes. Oxygen consumption by isolated mitochondria was measured using a Clark-type electrode. Liver (0.5 mg·mL^{-1}) or brain (0.3 mg·mL^{-1}) mitochondria were incubated in respiration medium [225 mM mannitol, 75 mM sucrose, 10 mM KCl, 20 mM Hepes, 5 mM KH_2PO_4, 0.5 mM EGTA, 3 mM $MgSO_4$, 0.3% fatty acid–free BSA (pH 7.4) at 37 °C]. Five mM glutamate and 5 mM malate were used as complex I substrates. ADP (2,000 nmol) was added to stimulate maximal respiration, or 400 nmol of ADP was included to determine the state 3 and state 4 respiration rates.

Rate of synaptosomal oxygen consumption was determined with the Seahorse XF24 instrument (Seahorse Bioscience) as described previously (7), using 30 μg of synaptosomes.

Maintenance of ATP Levels in Synaptosomes. ATP measurements were conducted as published (11) with the following modifications. Synaptosomes (0.5 mg·mL^{-1}) were incubated in incubation medium [3.5 mM KCl, 120 mM NaCl, 1.3 mM $CaCl_2$, 0.4 mM KH_2PO_4, 1.2 mM Na_2SO_4, 2 mM $MgSO_4$, 15 mM D-glucose, 2 mM pyruvate, 4 mg/mL BSA (pH 7.4) at 37 °C] for 5 min at 37 °C. Two 50-μL aliquots were prepared for each experiment. For the first, an additional 50 μL of incubation media was added, and the ATP was extracted immediately at time 0. For the second, 50 μL of incubation buffer was added, and the sample was incubated for a further 15 min at 37 °C. To determine the effects of increased synaptosome ATP consumption, 5 μM veratridine, 40 mM KCl, or 1 mM 4-aminopyridine were included in the incubation medium in some samples. The reaction was stopped, and the ATP was extracted from each aliquot by the addition of 5 μL of 6.5 M perchloric acid, centrifugation, and neutralization with 100 μL of 2 M Tris-acetate (pH 7.75). Following ATP extraction, 10 μL of the extract was added to 100 μL of luciferin/luciferase ENLITEN reagent (Promega), and the ATP levels were determined immediately using a standard curve. The ability of synaptosomes to maintain ATP levels was determined by comparing the ATP levels after an initial 5 min of incubation and after 15 min of incubation.

Measurement of Mitochondrial ROS Generation. The rate of ROS generation was determined by measuring the rate of H_2O_2 efflux using Amplex red (Invitrogen). Mitochondria (0.05 mg·mL^{-1}) or 0.5 mg·mL^{-1} synaptosomes were incubated in incubation medium [125 mM KCl, 20 mM Hepes, 2 mM K_2HPO_4, 1 mM $MgCl_2$, 0.1 mM EGTA, 0.025% BSA (pH 7.0) at 37 °C]. Glutamate (5 mM) and 5 mM malate were used to induce forward electron transfer. In reverse electron transfer experiments, 5 mM succinate and

1 μg·mL^{-1} oligomycin were included. To measure H_2O_2 in synaptosomes, 0.5 mg·mL^{-1} synaptosomes were incubated in incubation medium [3.5 mM KCl, 120 mM NaCl, 1.3 mM $CaCl_2$, 0.4 mM KH_2PO_4, 1.2 mM Na_2SO_4, 2 mM $MgSO_4$, 15 mM D-glucose, 4 mg/mL BSA (pH 7.0) at 37 °C]. Rotenone (4 μM) was added when necessary. Amplex red (1 μM) and 5 U·mL^{-1} horseradish peroxidase were added to initiate the reaction. The amount of hydrogen peroxide generated was determined using a H_2O_2 standard curve performed in the presence of unenergized mitochondria to account for quenching.

Immunoblotting. For mouse fibroblasts, Western blotting was performed with 10 μg of mitochondrial protein. The Mitoprofile Mixture, Grim19, and porin antibodies were purchased from Mitosciences. NDUFS8 (23 kDa) and NDUFS2 (49 kDa) antibodies were provided by Joel Lunardi (Laboratoire de Biochimie et Génétique Moléculaire, Grenoble, France), and MWFE antibody was provided by Immo Scheffler (Department of Biology, University of California, San Diego, CA).

For mouse tissue lysates, the mice were euthanized by cervical dislocation, and the brains were placed immediately into radioimmunoprecipitation assay (RIPA) buffer supplemented with protease inhibitor mixture (Sigma). The brains were homogenized on ice using an Omni Tissue Homogenizer (Omni), and gel electrophoresis and Western blotting were performed by standard procedures, with the blot analyzed using the Odyssey system. Complex I, II, and III antibodies were purchased from Mitosciences. β-Actin antibody was purchased from Abcam; 3-nitrotyprosine and GFAP antibodies were purchased from EMD and Dako, respectively.

Statistical Analysis. Statistical analyses were performed using the Graphpad Prism software. Two groups were compared using two-tailed *t* tests, with *P* values of <0.05 considered significant.

1. Trounce IA, Kim YL, Jun AS, Wallace DC (1996) Assessment of mitochondrial oxidative phosphorylation in patient muscle biopsies, lymphoblasts, and transmitochondrial cell lines. *Methods Enzymol* 264:484–509.
2. Fan W, Lin CS, Potluri P, Procaccio V, Wallace DC (2012) mtDNA lineage analysis of mouse L-cell lines reveals the accumulation of multiple mtDNA mutants and intermolecular recombination. *Genes Dev* 26(4):384–394.
3. Milakovic T, Johnson GV (2005) Mitochondrial respiration and ATP production are significantly impaired in striatal cells expressing mutant huntingtin. *J Biol Chem* 280 (35):30773–30782.
4. Sadun AA, Win PH, Ross-Cisneros FN, Walker SO, Carelli V (2000) Leber's hereditary optic neuropathy differentially affects smaller axons in the optic nerve. *Trans Am Ophthalmol Soc* 98:223–232.
5. Chen Q, Vazquez EJ, Moghaddas S, Hoppel CL, Lesnefsky EJ (2003) Production of reactive oxygen species by mitochondria: Central role of complex III. *J Biol Chem* 278(38): 36027–36031.
6. Sims NR, Anderson MF (2008) Isolation of mitochondria from rat brain using Percoll density gradient centrifugation. *Nat Protoc* 3(7):1228–1239.
7. Choi SW, et al. (2011) Intrinsic bioenergetic properties and stress sensitivity of dopaminergic synaptosomes. *J Neurosci* 31(12):4524–4534.
8. Dunkley PR, Jarvie PE, Robinson PJ (2008) A rapid Percoll gradient procedure for preparation of synaptosomes. *Nat Protoc* 3(11):1718–1728.
9. Grivennikova VG, Kapustin AN, Vinogradov AD (2001) Catalytic activity of NADH-ubiquinone oxidoreductase (complex I) in intact mitochondria. evidence for the slow active/inactive transition. *J Biol Chem* 276(12):9038–9044.
10. Ji F, et al. (2012) Mitochondrial DNA variant associated with Leber hereditary optic neuropathy and high-altitude Tibetans. *Proc Natl Acad Sci USA* 109(19): 7391–7396.
11. Kilbride SM, Telford JE, Tipton KF, Davey GP (2008) Partial inhibition of complex I activity increases Ca-independent glutamate release rates from depolarized synaptosomes. *J Neurochem* 106(2):826–834.

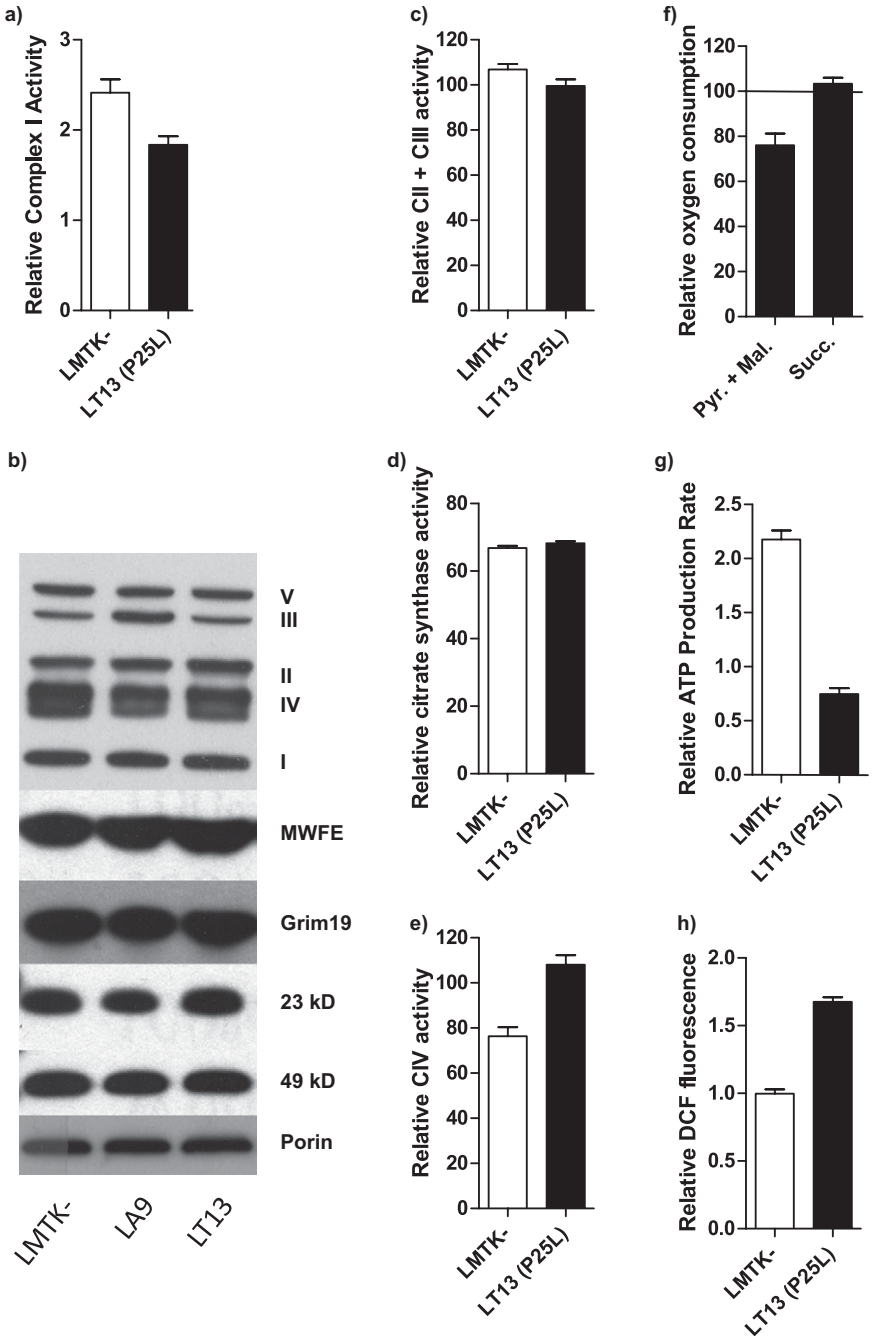

Fig. S1. Biochemical and immunoblotting assessments on the fibroblast cybrid harboring the *ND6* mutation. (*A*) Relative complex I–specific activity showing a 23% reduction in complex I activity in the mutant fibroblast cells ($P = 0.1294$). (*B*) Abundance of the respiratory complexes from the parental (LMTK$^-$) cells, LA9 cells, and the LT13 cell line, which harbors the P25L mutation in *ND6*. (*C*) Complex II plus III activity in wild-type (LMTK$^-$) and P25L mutant (LT13) cells. (*D*) Citrate synthase activity in wild-type (LMTK$^-$) and P25L (LT13) cells. (*E*) Complex IV activity in wild-type (LMTK$^-$) and *ND6* P25L (LT13) cells. The LT13 cells had a 30.9% increase in activity ($P = 0.053$). (*F*) Oxygen consumption in LT13 cells as a percentage of control cells (LMTK$^-$), using either complex I (pyruvate and malate) or complex II (succinate) substrates. LT13 (P25L) cells had a 24% decrease ($P = 0.0158$) in complex I–mediated respiration. (*G*) Relative ATP production in LT13 (P25L) and LMTK$^-$ cells. Complex Idriven ATP synthesis was reduced by 65% in LT13 (P25L) cells ($P = 0.0069$). (*H*) DCFDA [2′,7′-dichlorofluorescein diacetate] to monitor ROS generation in LT13 and LMTK$^-$ cells. *ND6* mutant cells produced 48% more fluorescence than the LMTK$^-$ control ($P < 0.0001$). $n = 3$ for both LMTK$^-$ control and LT13 mutant in all biochemical measurements other than *H*, in which $n = 5$.

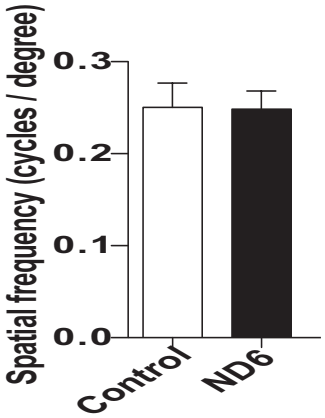

Fig. S2. Visual acuity of the *ND6* mice compared with controls. Optikinetics analysis, measured by the OptoMotry System, was determined by the effectiveness of mice tracking a rotating lined cylinder (n = 6 control mice; n = 8 ND6 mice).

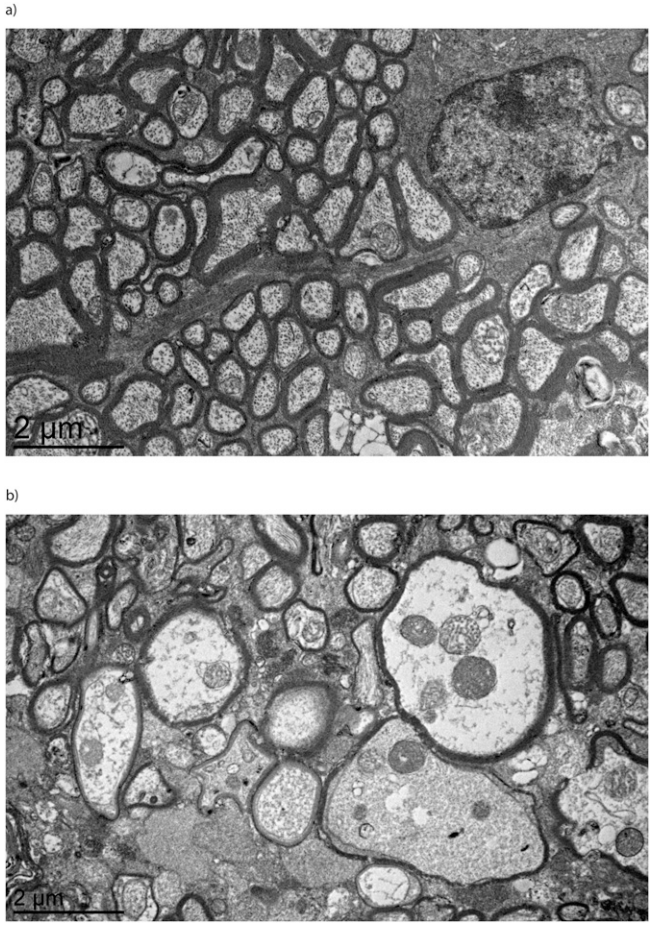

Fig. S3. Ultrastructural analysis of RGC axonal morphology in 24-mo-old *ND6* mutant mice. Electron microscopic images of retrobulbar optic nerves of 24-mo-old wild-type (*A*) and *ND6* mutant (*B*) mice at 2,000× magnification. RGC axons in ND6 mutant mice were much more swollen and irregular in diameters and shapes.

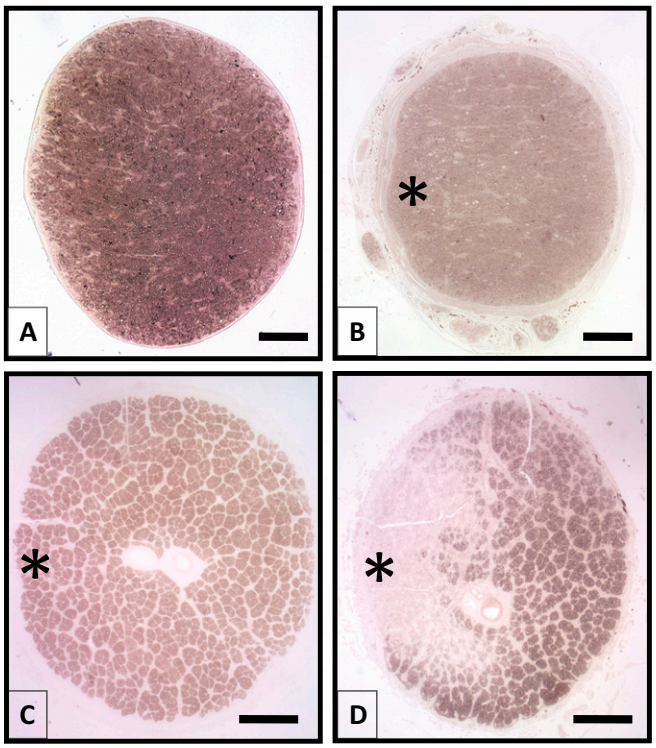

Fig. S4. Temporal distribution of axonal denegation in the optic nerve. Plastic embedded semithin sections of mouse (*A* and *B*) and human (*C* and *D*) retrobulbar optic nerves in cross-sectional profiles stained with *p*-phenylenediamine for myelin. (*A*) Wild-type mouse at 14 mo. (*B*) ND6 mutant mouse at 14 mo. Localized region of axonal swelling is oriented to the left (asterisk). (*C*) Human control (age, 58 y). Temporal aspect is oriented to the left (asterisk). (*D*) LHON patient (age, 52 y). Temporal region of axonal depletion is oriented to the left (asterisk). [Magnification: *A* and *B*, 200× (scale bars: 50 μm); *C* and *D*, 25× (scale bars: 500 μm).]

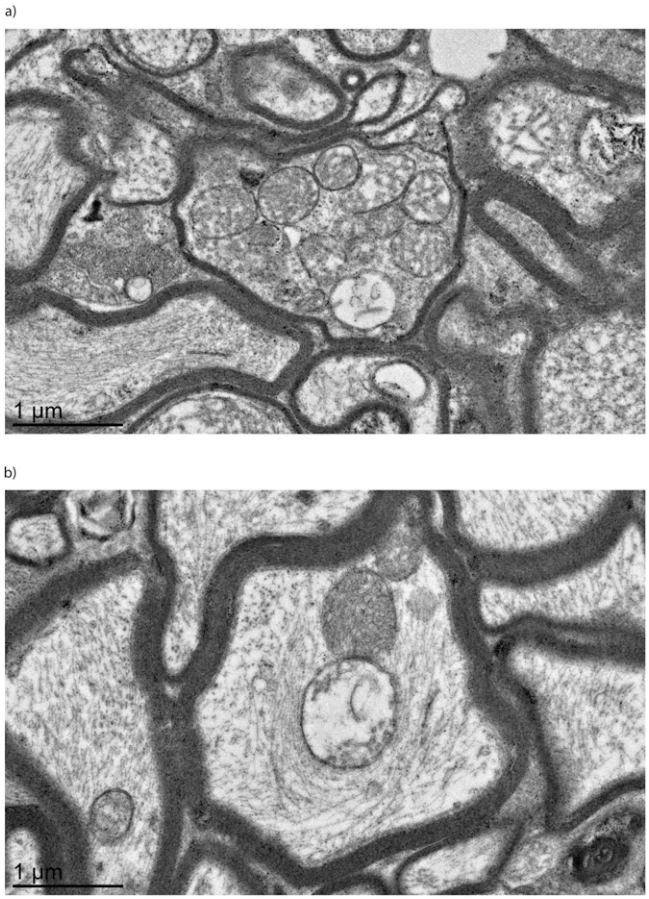

Fig. S5. Ultrastructural analysis of RGC axonal mitochondrial morphology in 24-mo-old ND6 mutant mice. Transmission electron microscopic images of 24-mo-old *ND6* mutant at 4,000× magnification indicating mitochondrial proliferation (*A*) and abnormal mitochondrial morphology (*B*).

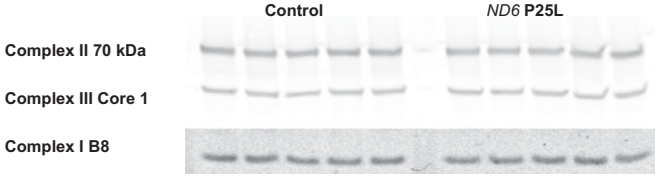

Fig. S6. Complex I, II, and III quantities in total forebrain lysates. Complex I, II, and III levels were determined by quantitative immunoblotting of representative subunits (n = 5; 10 μg of both control and ND6 mutant brain from independent extractions of whole cell lysates).

Table S1. Time to latency in ERG data

	Scotopic B wave			
Mouse strain	0.01 cd·s/m^2	1 cd·s/m^2	Scotopic A wave (1 cd·s/m^2)	Photopic B wave
Control	47.63 ± 3.052*	31.00 ± 0.4183*	18.88 ± 0.2562*	46.38 ± 0.8056*
ND6 (P25L)	55.56 ± 3.540* (P = 0.0998)	34.38 ± 1.599* (P = 0.0501)	21.13 ± 0.9784* (P = 0.0338)	47.64 ± 0.6429† (P = 0.2378)

All data are milliseconds ± SEM.
*n = 16.
$^\dagger n$ = 14.

Table S2. mtDNA polymorphisms in parental cell lines and derivatives

Position	Gene	Amino acid change	LMTK cell line*,†	*ND6* mutant mice	Lewis cell carcinoma cell line*,‡	A11 cell line§	C57BL/6J* mouse
9,348	*CoIII*	No change	A	A	G	G¶	G
9,818	$tRNA^{Arg}$	NA	AA	AA	A	A¶	A
13,997	*ND6*	P25L	G	A	G	A	G

NA, not applicable.

*mtDNA polymorphisms compiled by Bayona-Bafaluy et al. (1) and confirmed by in-house sequencing.

†Parental cell line used for mtDNA mutagenesis. $LMTK^-$ was originally derived from C3H/An mouse strain.

‡Parental cell line used to generate A11 cells harboring the same *ND6* mutation in Hashizume et al. (2). It was first derived from carcinoma of C57BL/6J mice.

§Cell line used to introduce the *ND6* mutation into mouse germ line as described in *Hashizume* et al. (2).

¶Predicted by assuming these positions are conserved in the A11 as the parental carcinoma cells.

1. Bayona-Bafaluy MP, Manfredi G, Moraes CT (2003) A chemical enucleation method for the transfer of mitochondrial DNA to rho(o) cells. *Nucleic Acids Res* 31(16):e98.
2. Hashizume O, et al. (2012) Specific mitochondrial DNA mutation in mice regulates diabetes and lymphoma development. *Proc Natl Acad Sci USA* 109(26):10528–10533.